sustainability

MDPI

Article

Effects of Material Composition and Curing Parameters on Performance of Cold Central Plant Recycled Cement-Stabilized Gravel

Jianfeng Jia [1,2,3], Le Cheng [4], Penghui Wen [4,*], Xuegang Zhang [1,2,3], Haiyan Li [1,2,3] and Chaohui Wang [4,*]

[1] Xinjiang Transportation Investment (Group) Co., Ltd., Urumqi 830000, China
[2] Xinjiang Transportation Investment Construction Management Co., Ltd., Urumqi 830000, China
[3] Key Laboratory of Transport Industry of Highway Engineering Technology in Arid Desert Areas, Urumqi 830000, China
[4] School of Highway, Chang'an University, Xi'an 710064, China
* Correspondence: 2019021008@chd.edu.cn (P.W.); wchh0205@chd.edu.cn (C.W.)

Abstract

To promote the large-scale recycling of reclaimed inorganic aggregates (RAI) generated from highway reconstruction projects, the effects of RAI content, reclaimed asphalt pavement (RAP) incorporation, RAI pretreatment, standing time, curing temperature, and curing mode on the performance of cold central plant recycled cement-stabilized gravel (CCSG) were investigated in this study. Scanning electron microscopy (SEM) and X-ray diffraction (XRD) were used to characterize microstructural changes. Increasing RAI content from 0% to 90% increased the optimum moisture content but slightly reduced the maximum dry density. Without RAP incorporation, the 7-day unconfined compressive strength (UCS), elastic modulus, and splitting tensile strength (STS) decreased by 30.34%, 21.29%, and 25.46%, respectively. Abrasion pretreatment and pozzolanic slurry strengthening improved mechanical performance. Compared with untreated CCSG, the latter increased the 28-day UCS, elastic modulus, and STS by 63.67%, 37.27%, and 64.77%, respectively. A 4-h standing period reduced the 7-day UCS and elastic modulus by 15.8% and 13.9%, respectively, while lowering the curing temperature from 20 °C to 5 °C reduced them by 26.9% and 18.8%, respectively. Abrasion pretreatment modified the surface morphology of RAI, whereas pozzolanic slurry strengthening formed a more continuous surface strengthening layer and denser bonding zones. These findings clarify the effects of RAI content, pretreatment, and preparation and curing parameters on the mechanical performance of CCSG.

Keywords: cold recycling; cement-stabilized gravel; material composition; curing parameters; RAI pretreatment; pavement performance

Check for updates

Academic Editors: Ling Xu, Fan Gu and Junfeng Gao

Received: 16 October 2026
Revised: 30 October 2026
Accepted: 3 November 2026
Published: 5 November 2026

Copyright: © 2026 by the authors. Licensee MDPI, Basel, Switzerland. This article is an open access article distributed under the terms and conditions of the Creative Commons Attribution (CC BY) license.

1. Introduction

Highway reconstruction and rehabilitation are important infrastructure activities driven by socioeconomic development demands. With the continuous improvement of the highway network in China, pavement maintenance, rehabilitation, and reconstruction projects have increased significantly in recent years. However, large quantities of reclaimed pavement materials are generated during these activities, mainly including reclaimed asphalt pavement (RAP) and reclaimed inorganic aggregates (RAI) [1–3]. Owing to the residual asphalt binder and relatively high recycling value of RAP, RAP recycling technologies have been extensively developed and widely applied. In contrast, the high-value

utilization of RAI remains at an early stage [4]. Compared with natural aggregates, RAI generally exhibits particle agglomeration and inferior mechanical properties. Under complex service environments involving freeze–thaw cycles, large temperature variations, and saline soils, RAI may contain considerable internal damage and abundant pores, which can adversely affect the performance of pavement base materials. Therefore, when natural aggregates are readily available, RAI is commonly used as embankment fill, while in some lower-grade pavement projects, it is reused in subbase layers through in situ cold recycling [5,6]. However, the widespread use of cement-stabilized materials in pavement base and subbase layers in China has led to the generation of substantial quantities of RAI during highway reconstruction. The high-value and large-scale recycling of RAI has therefore become an important technical challenge for transportation authorities and pavement engineers. Furthermore, under the current carbon peaking and carbon neutrality goals, natural aggregate extraction has been increasingly restricted in many regions. Consequently, the effective recycling and utilization of RAI provide a promising approach to alleviating aggregate resource shortages.

Current research on RAI recycling has mainly focused on in situ cold recycling and full-depth reclamation. Existing studies have primarily investigated the effects of material composition, RAI characteristics, and compaction methods on the performance of cold recycled materials. Tataranni et al. [7] conducted laboratory and field evaluations of recycled cement-bound mixtures and assessed the feasibility of incorporating 100% recycled cement-treated materials into pavement base layers, demonstrating their potential for pavement applications. Chakravarthi et al. [8] investigated the performance of cement-treated RAP and recycled concrete pavement materials and evaluated their applicability in pavement base layers. Li et al. [9] compared the mechanical properties and pavement performance of lime-fly ash-stabilized cold recycled macadam mixtures and found that their freeze–thaw resistance was comparable to that of cement-stabilized materials. Zhang et al. [10] evaluated the feasibility of recycling existing pavement subbase materials by investigating the mix design and pavement performance of cement-stabilized cold recycled lime soil. Ji et al. [11] compared the mechanical behavior of cement-stabilized cold recycled mixtures prepared using vibratory and static compaction methods under different material conditions. Jiang et al. [12] investigated the effects of cement content, reclaimed material proportion, virgin aggregate content, and curing age on the STS of cement-stabilized cold recycled mixtures using vibratory-compacted specimens. Xu et al. [13] analyzed the effects of virgin aggregate replacement ratio and compaction method on the UCS and STS of cement-stabilized cold recycled mixtures and discussed the corresponding strength development mechanisms. Xu et al. [14] investigated the effect of cement content on the properties of asphalt emulsion-stabilized cold recycled mixtures and analyzed its influence on strength development and mechanical characteristics. Hu et al. [15] investigated the mechanical properties, stiffness, and flexibility of cold recycled cement-stabilized gravel base milling mixes containing foamed asphalt. Al-Ihekwaba et al. [16] evaluated the effects of mixture composition, including binders, recycled aggregates, stabilizers, and aggregate types, on the mechanical properties of engineered emulsion-stabilized cold recycled materials. Jin et al. [17] evaluated cold in-place recycled asphalt mixtures through laboratory testing and a field demonstration on a low-volume road in Michigan, examining their performance under freeze–thaw conditions and using mechanistic-empirical pavement design to predict field performance.

In addition to mechanical properties, several studies have investigated the durability of cement-stabilized cold recycled materials and attempted to improve their early-age cracking and fatigue resistance through fibers and other functional additives. Wang et al. [18] systematically evaluated the fatigue behavior of cement cold recycled mixtures containing RAP

from seasonally frozen regions and found that the proportions of reclaimed materials from different pavement layers markedly affected fatigue characteristics. Gao et al. [19] investigated the effects of hydroxypropyl methylcellulose (HPMC) on full-depth cold recycled mixtures stabilized with cement to improve bleeding resistance and construction workability, and reported an adverse effect of HPMC on UCS. Liu et al. [20] evaluated the effects of polypropylene fibers on the freeze–thaw resistance, drying-shrinkage cracking resistance, tensile strength, and compressive strength of cement-stabilized cold recycled mixtures in alpine regions. Ren et al. [21] investigated the effects of recycled aggregate composition and cement content on the mechanical properties and material design of cement-stabilized cold recycled mixtures prepared using road-milling materials. Zhao et al. [22] further evaluated their fatigue characteristics and established a fatigue prediction model considering recycled aggregate composition. Mou et al. [23] incorporated early-strength anti-cracking materials into recycled cement-stabilized macadam and clarified their effects on early strength development and drying shrinkage. Fedrigo et al. [24] evaluated the effects of cement content, RAP content, and curing time on the shrinkage behavior of cold recycled cement-treated mixtures containing asphalt pavement materials and found that finer recycled materials exhibited greater shrinkage potential. Li et al. [25] analyzed the fatigue performance of full-depth reclamation materials stabilized with Portland cement using a Weibull distribution model. Liu et al. [26] developed an uncertainty quantification method for fatigue-life prediction of cement-stabilized cold recycled mixtures.

Although considerable progress has been made in understanding cement-stabilized cold recycled materials, previous studies have mainly focused on material composition, mechanical properties, and durability, particularly the effects of recycled material content and cement content. Moreover, most studies have concentrated on in situ cold recycling and full-depth reclamation, whereas limited attention has been given to cold central plant recycling of reclaimed cement-stabilized materials. Compared with in situ recycling, central plant recycling requires more rigorous control of material composition, preparation, and performance. For RAI originating from cold and arid regions, deterioration during previous service may further impair its recycling performance. However, the effects of RAI content, RAI pretreatment, and preparation and curing parameters on the performance of cold central plant recycled cement-stabilized gravel (CCSG) remain insufficiently understood.

To address these research gaps, this study investigates the recycling of RAI obtained from reclaimed cement-stabilized gravel in cold and arid regions for the preparation of CCSG. The compaction characteristics of CCSG are first evaluated, followed by systematic investigation of the effects of RAI content and RAI pretreatment on its mechanical properties. The effects of preparation and curing parameters are then examined. In addition, scanning electron microscopy (SEM) and X-ray diffraction (XRD) are employed to clarify the microstructural mechanisms underlying the observed mechanical behavior. The findings provide experimental evidence on the effects of RAI content, pretreatment, and preparation and curing parameters on the mechanical performance of CCSG incorporating RAI recovered from cold and arid regions.

2. Materials and Methods

2.1. Materials

RAI was obtained from reclaimed cement-stabilized gravel generated during the milling of a typical arterial highway undergoing reconstruction and expansion in Xinjiang, China. Prior to testing, the RAI was air-dried and sieved to the required particle sizes. RAP was obtained from the milled asphalt surface layers of the same project, while locally sourced natural gravel from Xinjiang was used as the virgin aggregate. The appearances of

the different aggregate types are shown in Figure 1. The particle-size distribution curves of RAI, RAP, and virgin gravel obtained from sieve analysis are presented in Figure 2.

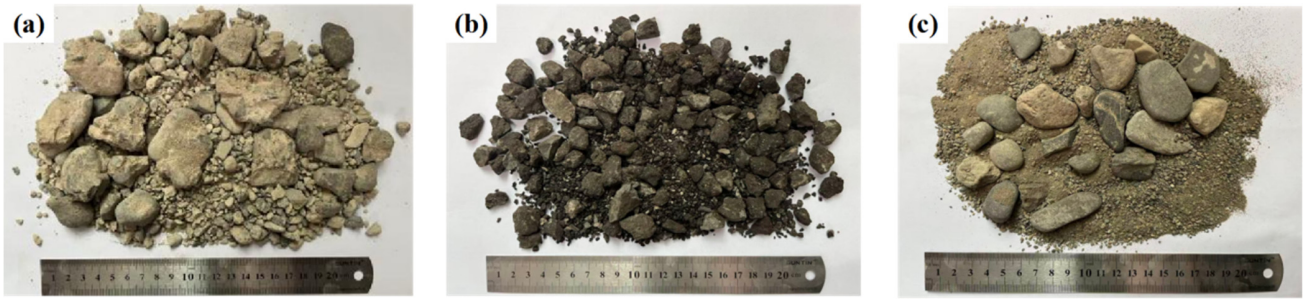


Figure 1. Appearance of aggregates: (**a**) RAI, (**b**) RAP, (**c**) gravel.

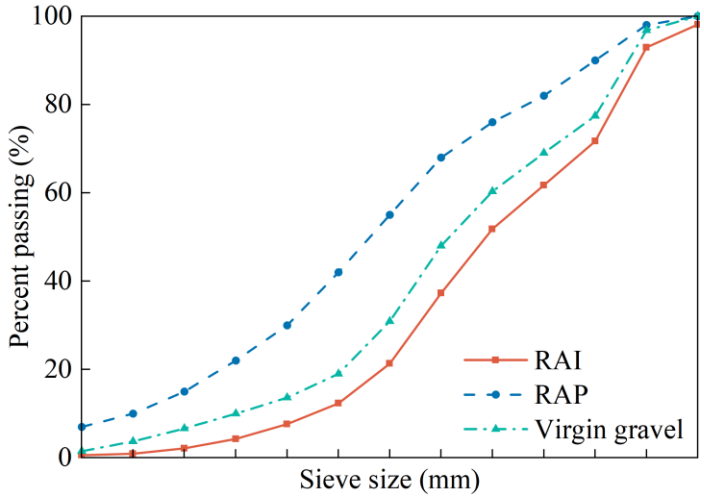


Figure 2. Particle-size distribution curves of RAI, RAP, and virgin gravel.

P·O 42.5 ordinary Portland cement was used as the binder. Two RAI pretreatment methods were adopted: Los Angeles abrasion pretreatment and pozzolanic slurry strengthening. The pozzolanic slurry was composed of steel slag powder (SSP), carbide slag (CS), ground granulated blast-furnace slag (GGBFS), and sodium silicate (SS), as shown in Figure 3.

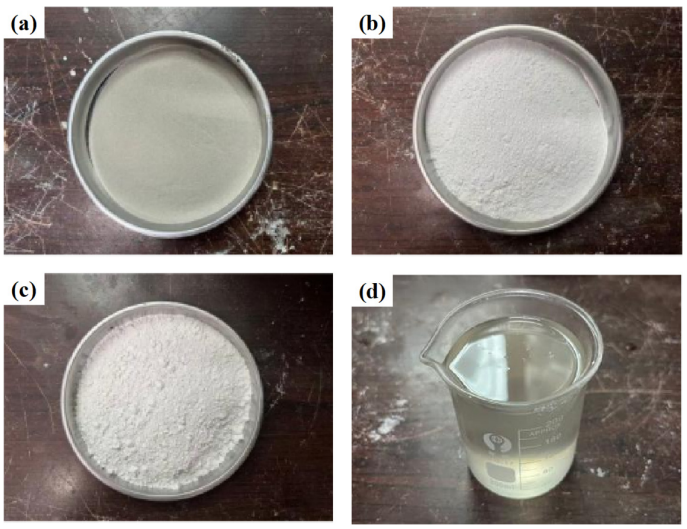


Figure 3. Components of the strengthening slurry: (**a**) SSP, (**b**) CS, (**c**) GGBFS, (**d**) SS.

2.2. Experimental Design

To clarify the effects of RAI content, RAI pretreatment, and preparation and curing parameters on the performance of CCSG, a systematic investigation was conducted in terms of compaction characteristics, mechanical properties, and microstructure, with particular emphasis on performance evolution and the underlying mechanisms. The overall experimental framework is illustrated in Figure 4.

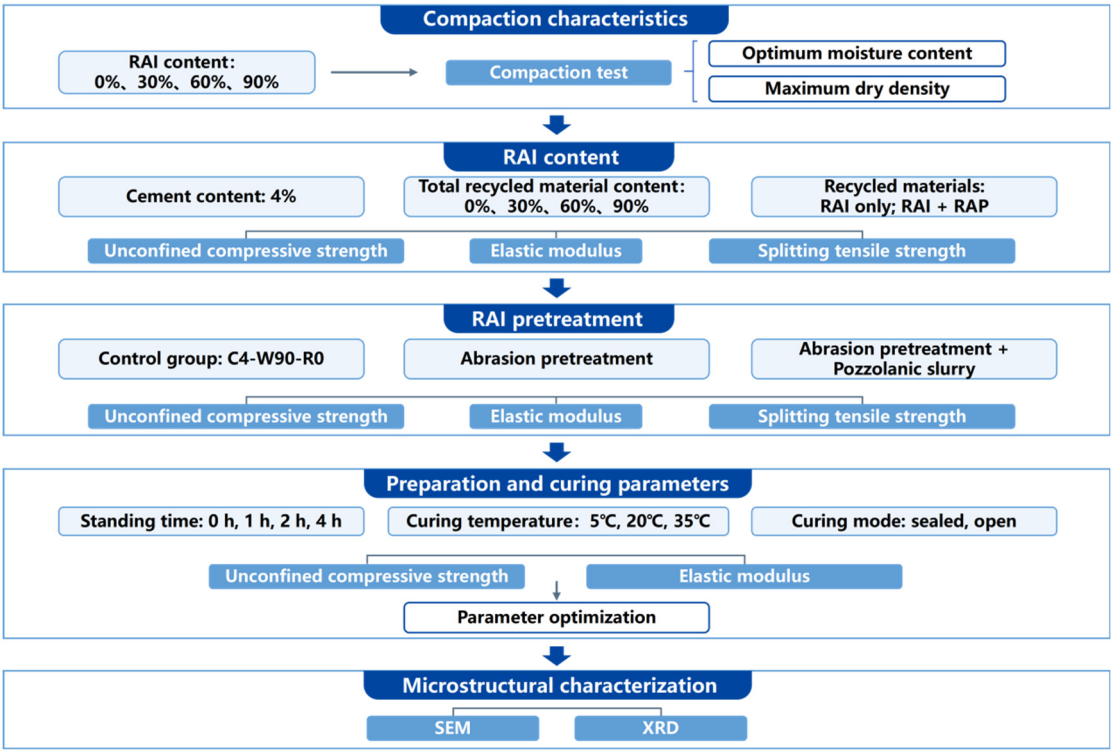


Figure 4. Experimental framework.

2.2.1. Compaction Testing

A cement content of 4% was adopted for the subsequent experiments based on local engineering practice and construction experience in Xinjiang. To determine the compaction characteristics of CCSG with different RAI contents, groups with RAI contents of 0%, 30%, 60%, and 90% were designed using this fixed cement content. The optimum moisture content and maximum dry density of each group were determined through compaction tests, and the experimental design is presented in Table 1. The group codes were defined in the form of "C-W-R", where C represents the cement content, W represents the total content of recycled materials, and R represents the proportion of RAP in the recycled materials. For instance, C4-W30-R50 denotes a group with 4% cement and a total recycled material content of 30%, comprising actual RAI and RAP contents of 15% each. The RAI and RAP contents were calculated relative to the total aggregate mass, excluding cement, while the cement content was calculated separately on the same basis.

Table 1. Experimental design for material composition.

No.	Group Code	Cement Content (%)	Total Recycled Material Content (%)	Actual RAI Content (%)	Actual RAP Content (%)
1	C4-W0-R0	4	0	0	0
2	C4-W15-R100		15	0	15
3	C4-W30-R0		30	30	0
4	C4-W30-R50		30	15	15
5	C4-W60-R0		60	60	0
6	C4-W60-R25		60	45	15
7	C4-W90-R0		90	90	0
8	C4-W90-R17		90	75	15
9	C4-W90-R0-A		90	90	0
10	C4-W90-R0-APS		90	90	0

2.2.2. Material Composition Design

To investigate the effects of RAI content, RAP incorporation, and RAI pretreatment on the mechanical properties of CCSG, the experimental program was designed at a fixed cement content of 4%, with the RAI content varied systematically and RAP introduced at an actual content of 15% in selected groups. Aggregate gradations were designed in accordance with the requirements of the Technical Specifications for Recycling of Asphalt Pavement (JTG/T 5521-2019) [27]. For different RAI and RAP contents, the proportions of individual aggregate size fractions were adjusted separately to determine the target gradation of each mixture. The C4-W90-R0 group was selected for RAI pretreatment. Two pretreatment methods were adopted: abrasion pretreatment and combined abrasion pretreatment with pozzolanic slurry strengthening. The corresponding groups were designated as C4-W90-R0-A and C4-W90-R0-APS, respectively. The UCS, elastic modulus, and STS of the different groups were compared, and the experimental design is presented in Table 2.

Table 2. Experimental design of preparation and curing parameters.

No.	Group Code	Standing Time (h)	Curing Temperature (°C)	Curing Mode
1	T0-20–SC	0	20	Sealed curing
2	T1-20–SC	1		
3	T2-20–SC	2		
4	T4-20–SC	4		
5	T0-5–SC	0	5	
6	T0-20–SC		20	
7	T0-35–SC		35	
8	T0-5–OC	0	5	Open curing
9	T0-20–OC		20	

2.2.3. Preparation and Curing Parameters

To investigate the effects of construction conditions on the performance of cement-stabilized cold recycled gravel, three parameters—standing time, curing temperature, and

curing mode—were investigated using the C4-W60-R0 mixture. The standing time was set to 0, 1, 2, and 4 h to simulate different transportation and waiting durations. The curing temperature was set at 20 °C as the reference condition, while 5 °C and 35 °C were selected to represent low-temperature and high-temperature construction environments, respectively. Two curing modes, namely sealed curing (SC) and open curing (OC), were adopted to evaluate differences in performance under different moisture-retention conditions. The T0-20–SC group served as the common reference condition for the standing-time and curing-temperature test series. The detailed experimental design is presented in Table 2.

2.2.4. Microstructural Testing

To characterize the interfacial bonding among recycled aggregates, virgin aggregates, and the cementitious matrix in CCSG and to elucidate the microstructural mechanisms governing strength development, SEM and XRD analyses were conducted on specimens subjected to different test conditions.

2.3. Test Methods

1. Compaction Test

The compaction test of CCSG was conducted in accordance with JTG 3441-2024 [28]. A multifunctional electric compactor was used, and the test procedure is illustrated in Figure 5. The wet density and dry density were calculated using Equations (1) and (2), respectively.

$$\rho_w = \frac{m_1 - m_2}{V} \tag{1}$$

where ρ_w is the wet density of CCSG (g/cm^3); m_1 is the total mass of the compaction mold and compacted wet specimen (g); m_2 is the mass of the compaction mold (g); and V is the volume of the compaction mold (cm^3).

$$\rho_d = \frac{\rho_w}{1 + 0.01w} \tag{2}$$

where ρ_d is the dry density of CCSG (g/cm^3), and w is the moisture content of CCSG expressed as a percentage (%).

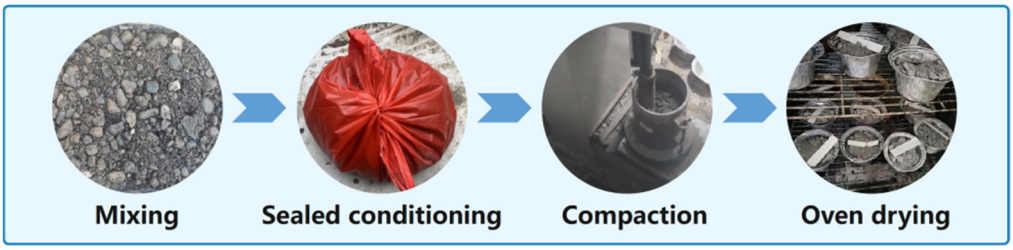


Figure 5. Compaction test procedure.

2. UCS Test

The UCS test of CCSG was conducted in accordance with JTG 3441-2024. The constituent materials of each group were thoroughly mixed according to the designed proportions at the corresponding OMC and then statically compacted into cylindrical specimens (150 mm in diameter and height) at a target degree of compaction of 98% of the corresponding MDD. After demolding, the actual dry density and degree of compaction were calculated from the measured specimen mass and dimensions. All specimens met the allowable deviation of ±1 percentage point from the target degree of compaction. The specimens were then demolded and cured under constant-temperature and constant-humidity conditions. During the final 24 h of the specified curing period, the specimens were immersed in

water. Before testing, the specimens were removed from the water and the surface water was wiped off. A universal testing machine (UTM) was used to apply a continuous compressive load at a loading rate of 1 mm/min until failure. The peak load was recorded, and the UCS was calculated using Equation (3).

$$R_c = \frac{P}{A} \tag{3}$$

where R_c is the UCS (MPa); P is the peak compressive load (N); A is the cross-sectional area of the specimen (mm^2), calculated as $A = \frac{1}{4}\pi D^2$; and D is the specimen diameter (mm).

3. Elastic Modulus Test

The elastic modulus test of CCSG was conducted in accordance with JTG D50-2017 [29]. Specimen preparation and curing followed the same procedures as those used for the UCS test. After curing, an extensometer with an initial gauge length of 100 mm was mounted at the mid-height of the cylindrical specimen to measure axial deformation. Before testing, the specimen was centered between the upper and lower loading platens of the UTM, and a preload of 50 N was applied to ensure full contact between the specimen and the platens. The specimen was then continuously loaded at a rate of 1 mm/min until failure. The peak load and axial strain were recorded, and the strain corresponding to 30% of the peak load was determined from the load-strain curve. The elastic modulus was calculated using Equation (4). The test procedure is shown in Figure 6.

$$E = \frac{1.2F_r}{\pi D^2 \varepsilon_3} \tag{4}$$

where E is the elastic modulus (MPa); F_r is the peak compressive load (N); D is the specimen diameter (mm); and ε_3 is the axial strain corresponding to 30% of the peak compressive load (dimensionless).

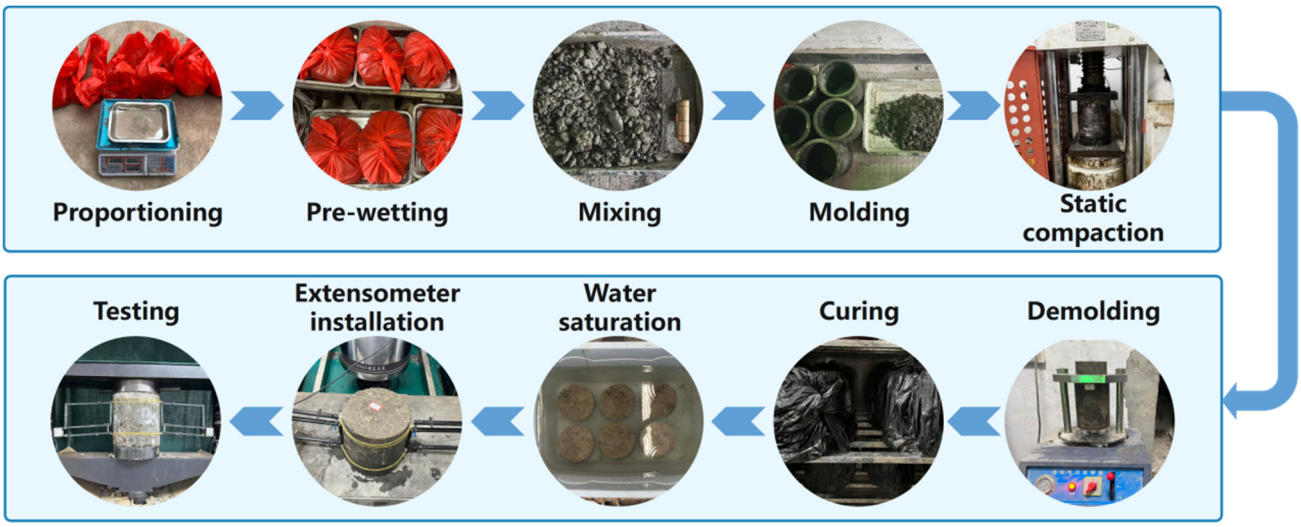


Figure 6. Elastic modulus test procedure.

4. STS Test

The STS test of CCSG was conducted in accordance with JTG 3441-2024. Specimen preparation and curing followed the same procedures as those used for the UCS test. After curing, the cylindrical specimen was placed horizontally between the upper and lower loading platens of the UTM and continuously loaded at a rate of 1 mm/min until splitting failure. The peak splitting load was recorded, and the STS was calculated using Equation (5).

$$R_s = \frac{2P}{\pi dh} \tag{5}$$

where R_s is the STS (MPa); P is the peak splitting load (N); d is the specimen diameter (mm); and h is the height of the water-saturated specimen (mm).

5. RAI Pretreatment Test

Two RAI pretreatment methods were adopted: abrasion pretreatment and abrasion pretreatment followed by pozzolanic slurry strengthening. The abrasion-treated and abrasion-pozzolanic-slurry-strengthened groups were designated as A and APS, respectively. The abrasion pretreatment was performed using a Los Angeles abrasion machine with six steel balls for 400 revolutions. For the A group, the abraded RAI was subsequently sieved into different particle-size fractions and recombined according to the designed aggregate gradation before specimen preparation. For the combined treatment, RAI particles larger than 2.36 mm were first subjected to abrasion pretreatment and then strengthened with pozzolanic slurry. The strengthening slurry was prepared using SSP, GGBFS, CS, and SS at a mass ratio of 40:60:4:1, with a slurry-to-RAI mass ratio of 1:8. After slurry strengthening, RAI fine aggregates with particle sizes of 0–1.18 mm were added and thoroughly mixed. The detailed procedure is illustrated in Figure 7.



Figure 7. RAI pretreatment procedure.

6. Preparation and Curing Parameter Test

To investigate the effects of preparation and curing parameters on the mechanical properties of CCSG, standing time, curing temperature, and curing mode were varied systematically.

(1) Standing time was set to 0, 1, 2, or 4 h from the completion of mixing, with 0 h indicating immediate molding. During standing, loose mixtures were covered with plastic film and kept at ambient laboratory temperature and humidity, then briefly remixed before compaction.

(2) Curing temperature: Three curing temperatures of 5, 20, and 35 °C were adopted to represent low-temperature, standard, and high-temperature curing conditions, respectively.

(3) Curing mode: Two curing modes, SC and OC, were adopted. SC simulated moisture-retaining curing by wrapping the specimens with plastic film, whereas OC simulated field exposure with water spraying. The specimens were cured at 5 and 20 °C under both curing modes.

7. Microstructural Characterization

SEM was performed using a ZEISS Sigma 360 (Oberkochen, Germany) at 500× magnification, while XRD was conducted using a Bruker D8 ADVANCE (Karlsruhe, Germany) over a 2θ range of 5–80°, with a scanning step size of 0.02° and a scanning rate of 2°/min.

3. Results and Discussion

3.1. Compaction Characteristics

To clarify the effect of RAI content on the compaction characteristics of CCSG, the optimum moisture content (OMC) and maximum dry density (MDD) of each group were determined from the compaction test results obtained at different moisture contents. The results are presented in Figure 8.

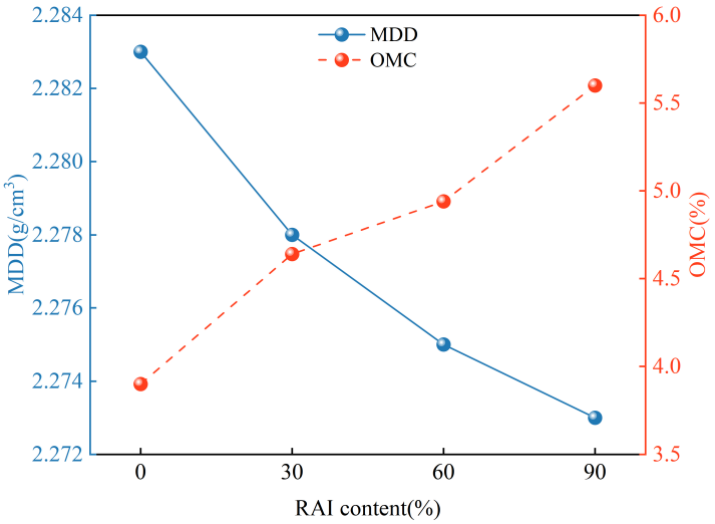


Figure 8. Compaction characteristics under different RAI contents.

As shown in Figure 8, the MDD of CCSG gradually decreased with increasing RAI content, although the overall reduction was relatively limited. In contrast, the OMC showed a pronounced increasing trend, with a maximum increase of 43.6%. The decrease in MDD can be attributed primarily to the damage and fragmentation of RAI during long-term service and milling, which generate abundant microcracks and internal pores. Compared with natural gravel, RAI has a lower packing density; therefore, increasing its content reduces the overall compactness of the aggregate skeleton and consequently lowers the MDD. In addition, the porous and rough surface of RAI, together with the adhered residual mortar, increases water demand. As the RAI content increases, more water is required to fill internal voids and provide sufficient lubrication between particles during compaction, resulting in a marked increase in the OMC.

3.2. Effect of RAI Content on Mechanical Properties

To investigate the effect of RAI content on the mechanical properties of CCSG, the UCS, elastic modulus, and STS were evaluated under conditions without RAP and with RAP incorporated at an actual content of 15%. The 7-day and 28-day UCS results at different RAI contents are presented in Figure 9. As shown in Figure 9a, without RAP incorporation, increasing the RAI content from 0% to 90% decreased the 7-day and 28-day UCS of CCSG from 4.92 and 6.64 MPa to 3.43 and 4.90 MPa, respectively, corresponding to reductions of 30.34% and 26.33%. The greater reduction at 7 days indicates that the adverse effect of RAI was more pronounced at early curing ages. This reduction can be attributed to the increasing amount of adhered residual mortar and associated interfacial transition zones introduced with higher RAI contents. The pores and pre-existing defects within the residual mortar, together with the relatively weak interfaces between the residual mortar and newly formed cementitious matrix, promote local stress concentration and disrupt load transfer, thereby reducing the UCS [30,31]. At 28 days, continued hydration further densified the

cementitious matrix and strengthened interfacial bonding, partially compensating for these defects and resulting in a smaller reduction in UCS.

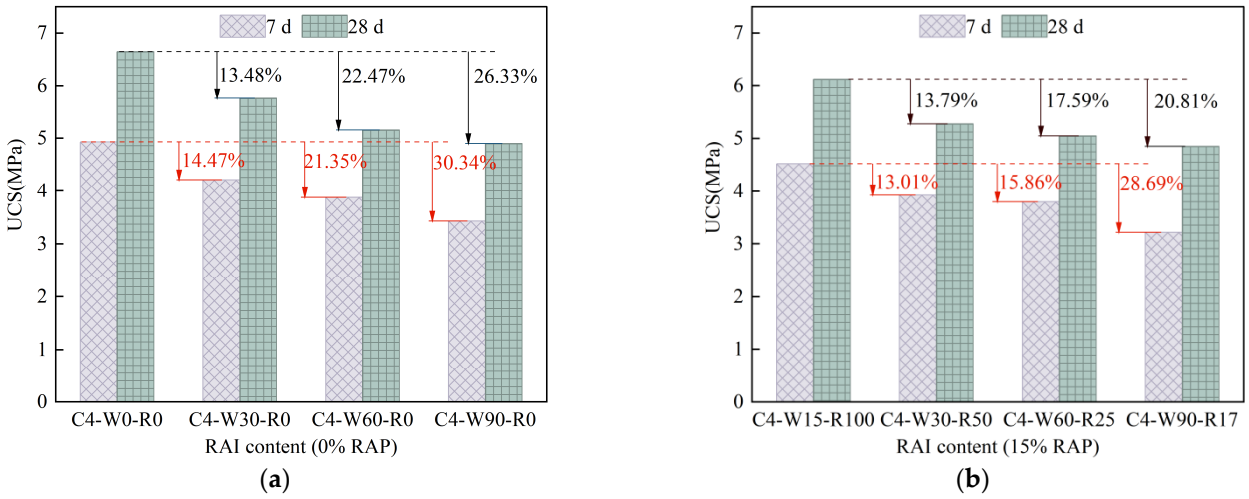


Figure 9. Effect of RAI content on UCS: (**a**) without RAP incorporation. (**b**) with RAP incorporation.

According to the 7-day strength requirements for cement-stabilized materials used in expressway and Class I highway base courses specified in JTG D50-2017, the groups with RAI contents of 0% and 30% satisfied the requirements for base-course applications. In contrast, the groups with RAI contents of 60% and 90% met only the requirements for subbase applications, indicating that further performance enhancement is required before CCSG with high RAI contents can be used in base courses.

As shown in Figure 9b, with the actual RAP content fixed at 15%, increasing the actual RAI content from 0% to 75% decreased the 7-day and 28-day UCS from 4.51 and 6.12 MPa to 3.22 and 4.85 MPa, respectively, corresponding to reductions of 28.69% and 20.81%. The greater reduction at 7 days indicates that early-age strength was more sensitive to the increasing content of recycled materials. In addition to the weak interfaces introduced by RAI, the aged asphalt film coating the RAP surface reduces direct contact between the aggregates and the newly formed cementitious matrix, resulting in a more porous and weakly bonded interfacial region [32,33]. Moreover, organic components in the asphalt film may inhibit cement hydration, further limiting the early-age strength development of RAP-containing CCSG [34].

The 7-day and 28-day elastic modulus results at different RAI contents are presented in Figure 10. As shown in Figure 10a, without RAP incorporation, increasing the RAI content from 0% to 90% decreased the 7-day and 28-day elastic modulus of CCSG from 6491 and 7425 MPa to 5109 and 6442 MPa, respectively, corresponding to reductions of 21.29% and 13.24%. The smaller reduction at 28 days indicates that the adverse effect of RAI on stiffness became less pronounced with increasing curing age. This can be attributed to continued hydration and enhanced interfacial bonding at later ages, which increased interparticle restraint and partially compensated for the stiffness loss. Compared with natural gravel, the adhered residual mortar in RAI has a lower stiffness. As the RAI content increases, the contribution of high-stiffness aggregates to the load-bearing skeleton decreases, leading to greater deformation of the particle skeleton under loading and consequently a lower macroscopic elastic modulus [31].

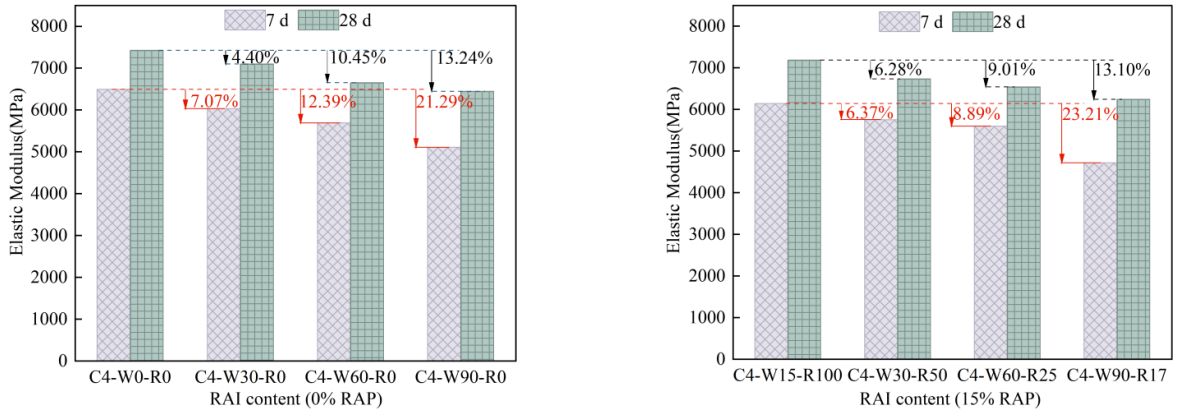


Figure 10. Effect of RAI content on elastic modulus: (**a**) without RAP incorporation. (**b**) with RAP incorporation.

As shown in Figure 10b, with the actual RAP content fixed at 15%, increasing the actual RAI content from 0% to 75% decreased the 7-day and 28-day elastic modulus from 6143 and 7185 MPa to 4717 and 6241 MPa, respectively, corresponding to reductions of 23.21% and 13.10%. The greater reduction at 7 days again indicates a stronger adverse effect at early curing ages. With the combined incorporation of RAI and RAP, the proportion of relatively low-stiffness recycled components increases further. In particular, the aged asphalt film coating the RAP surface is more deformable and weakens interparticle restraint within the load-bearing skeleton. Consequently, local deformation and strain concentration are more likely to develop under loading, resulting in a progressive decrease in elastic modulus.

The 7-day and 28-day STS results at different RAI contents are presented in Figure 11. As shown in Figure 11a, without RAP incorporation, increasing the RAI content from 0% to 90% decreased the 7-day and 28-day STS of CCSG from 0.422 and 0.651 MPa to 0.315 and 0.481 MPa, respectively, corresponding to reductions of 25.46% and 26.11%. The comparable reductions at the two curing ages indicate that the adverse effect of RAI on splitting resistance persisted with curing age. Splitting failure is governed primarily by interparticle bonding and crack propagation. As the RAI content increases, more adhered residual mortar and pre-existing damaged zones are introduced, facilitating the initiation and propagation of tensile cracks around recycled aggregates and consequently reducing resistance to splitting failure [31]. Although continued hydration improves the overall bonding strength at later ages, it cannot fully compensate for the inherent defects of recycled aggregates, which explains why the reduction in 28-day STS remained comparable to that at 7 days.

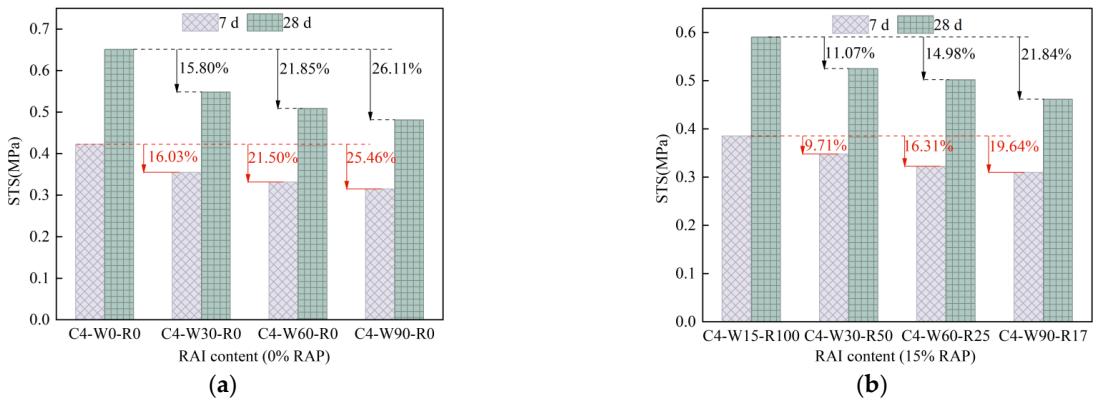


Figure 11. Effect of RAI content on STS: (**a**) without RAP incorporation. (**b**) with RAP incorporation.

As shown in Figure 11b, with the actual RAP content fixed at 15%, increasing the actual RAI content from 0% to 75% decreased the 7-day and 28-day STS from 0.385 and 0.590 MPa to 0.310 and 0.461 MPa, respectively, corresponding to reductions of 19.64% and 21.84%. A similar decreasing trend was observed under RAP incorporation. With the combined incorporation of RAI and RAP, adhered residual mortar and asphalt-coated particles coexist within the material. The aged asphalt film provides relatively weak interfacial restraint, hindering effective tensile stress transfer and promoting crack propagation around recycled particles. Consequently, increasing the total recycled material content progressively reduces the splitting resistance of CCSG, and this adverse effect remains evident at later curing ages.

3.3. Effect of RAI Pretreatment on Mechanical Properties

To evaluate the effectiveness of RAI pretreatment, the mechanical properties of the A and APS groups were compared with those of the untreated C4-W90-R0 control group.

The 7-day and 28-day UCS results under different RAI pretreatment conditions are presented in Figure 12. As shown in Figure 12, compared with the untreated C4-W90-R0 control group, the A group increased the 7-day and 28-day UCS from 3.43 and 4.90 MPa to 4.56 and 6.53 MPa, respectively, corresponding to increases of 32.86% and 33.41%. This improvement may be associated with the altered RAI surface morphology and enhanced particle interlocking, contributing to a more stable load-bearing skeleton under compression.

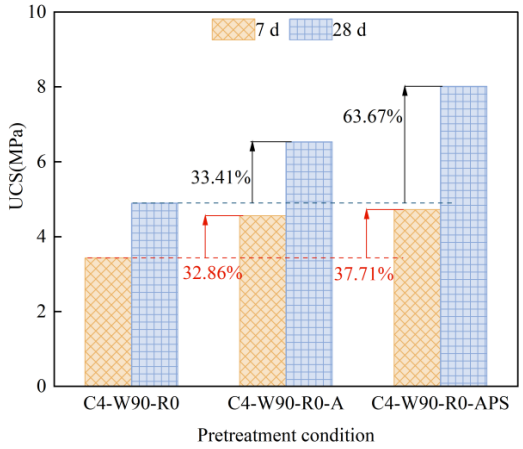


Figure 12. Effect of RAI pretreatment on UCS.

The APS group further increased the 7-day and 28-day UCS to 4.72 and 8.01 MPa, respectively, representing increases of 37.71% and 63.67% relative to the untreated control group. Compared with the A group, the additional increase in 7-day UCS was only 3.51%, whereas the 28-day UCS increased by 22.66%, indicating a more pronounced later-age strengthening effect. This can be attributed to the alkaline environment and soluble silica provided by carbide slag and sodium silicate, which promote the continued reaction of reactive silicate and aluminate phases in steel slag powder and GGBFS, leading mainly to the formation of C-A-S-H gels [35]. These reaction products fill surface defects and strengthen interfacial bonding. As the reactions proceed, the surface strengthening layer and interfacial zones become progressively denser, resulting in a greater strengthening effect at 28 days than at 7 days.

Further comparison showed that the 28-day UCS of the A group reached 6.53 MPa, which was close to that of the C4-W0-R0 control group containing only virgin aggregate (6.64 MPa). The 28-day UCS of the APS group further increased to 8.01 MPa, exceeding that of the C4-W0-R0 group by 20.63%. These results indicate that abrasion pretreatment can substantially restore the load-bearing capacity of CCSG with a high RAI content, while

abrasion pretreatment followed by pozzolanic slurry strengthening provides further later-age strength enhancement. According to the strength requirements for base materials specified in JTG D50-2017, the 7-day UCS values of the A and APS groups were 4.56 and 4.72 MPa, respectively, both exceeding 4.0 MPa and satisfying the strength requirement for base-course applications under heavy traffic conditions. Therefore, appropriate RAI pretreatment and surface strengthening can effectively mitigate the adverse effects associated with high RAI incorporation and support the high-value utilization of RAI in cold recycled cement-stabilized pavement bases.

The 7-day and 28-day elastic modulus results under different RAI pretreatment conditions are presented in Figure 13. As shown in Figure 13, compared with the untreated C4-W90-R0 control group, the A group increased the 7-day and 28-day elastic modulus from 5109 and 6442 MPa to 6258 and 7326 MPa, respectively, corresponding to increases of 22.49% and 13.72%. The APS group further increased the elastic modulus to 6779 and 8843 MPa, representing increases of 32.69% and 37.27% relative to the untreated control group. Compared with the A group, the APS group provided additional increases of 8.33% and 20.71% at 7 and 28 days, respectively, indicating a more pronounced later-age stiffness enhancement.

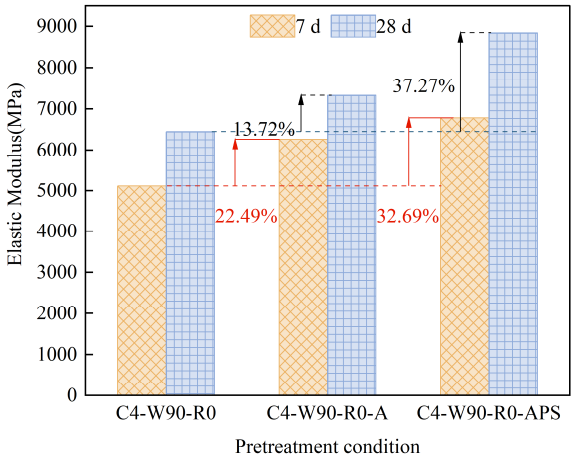


Figure 13. Effect of RAI pretreatment on elastic modulus.

The increase may be related to improved particle contact and interfacial bonding, facilitating stress transfer through the cement-stabilized aggregate skeleton. Following pozzolanic slurry strengthening, the surface strengthening layer and denser interfacial regions provide greater restraint against particle deformation. As the strengthening reactions proceed with curing age, this restraint becomes progressively stronger, reducing local compressive deformation and leading to a greater increase in elastic modulus at 28 days than at 7 days [35]. Overall, both pretreatment methods improved the stiffness of CCSG, while the APS group exhibited the strongest later-age stiffness gain, with a 28-day elastic modulus of 8843 MPa.

The 7-day and 28-day STS results under different RAI pretreatment conditions are presented in Figure 14. As shown in Figure 14, both the A and APS groups exhibited markedly higher STS than the untreated C4-W90-R0 control group. The A group increased the 7-day and 28-day STS to 0.399 and 0.646 MPa, respectively, corresponding to increases of 26.79% and 34.37%. The APS group further increased the STS to 0.448 and 0.793 MPa, representing overall increases of 42.25% and 64.77% relative to the untreated control group. Compared with the A group, the APS group provided additional increases of 12.20% and 22.62% at 7 and 28 days, respectively. The greater improvement at 28 days indicates that the

surface strengthening effect became more pronounced with curing age, leading to enhanced later-age resistance to tensile cracking.

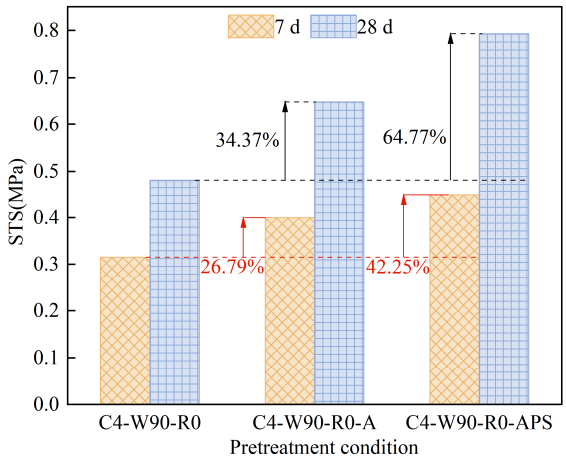


Figure 14. Effect of RAI pretreatment on STS.

The improvement may be associated with enhanced interfacial contact between RAI and the cementitious matrix, facilitating stress transfer across particle–matrix interfaces under tensile loading. Following pozzolanic slurry strengthening, secondary cementitious reactions at the aggregate surface further enhance interfacial bonding, promote more effective tensile stress transfer between particles, and consequently delay crack initiation and propagation [36].

3.4. Effects of Preparation and Curing Parameters

Considering the pronounced seasonal temperature variations and practical construction conditions in Xinjiang, the effects of standing time, curing temperature, and curing mode on the mechanical properties of CCSG were investigated to identify appropriate preparation and curing parameters.

3.4.1. Standing Time

The 7-day and 28-day UCS and elastic modulus results at different standing times are presented in Figure 15. As shown in Figure 15a,b, both the UCS and elastic modulus of CCSG decreased with increasing standing time. Under immediate compaction, the 7-day and 28-day UCS were 3.87 and 5.15 MPa, respectively. After standing for 2 h, the corresponding reductions were only 4.2% and 4.3%, whereas extending the standing time to 4 h increased the reductions to 15.8% and 11.5%, respectively. This indicates that the adverse effect of delayed compaction became more pronounced when the standing time exceeded 2 h. A similar trend was observed for the elastic modulus. The 7-day and 28-day elastic modulus decreased from 5687 and 6649 MPa under immediate compaction to 4896 and 5942 MPa after 4 h of standing, corresponding to reductions of 13.9% and 10.6%, respectively. Notably, after 2 h of standing, the 7-day UCS decreased by only 4.2%, whereas the elastic modulus decreased by 8.2%, indicating that stiffness was more sensitive than strength to changes in particle contact and compaction state induced by delayed compaction.

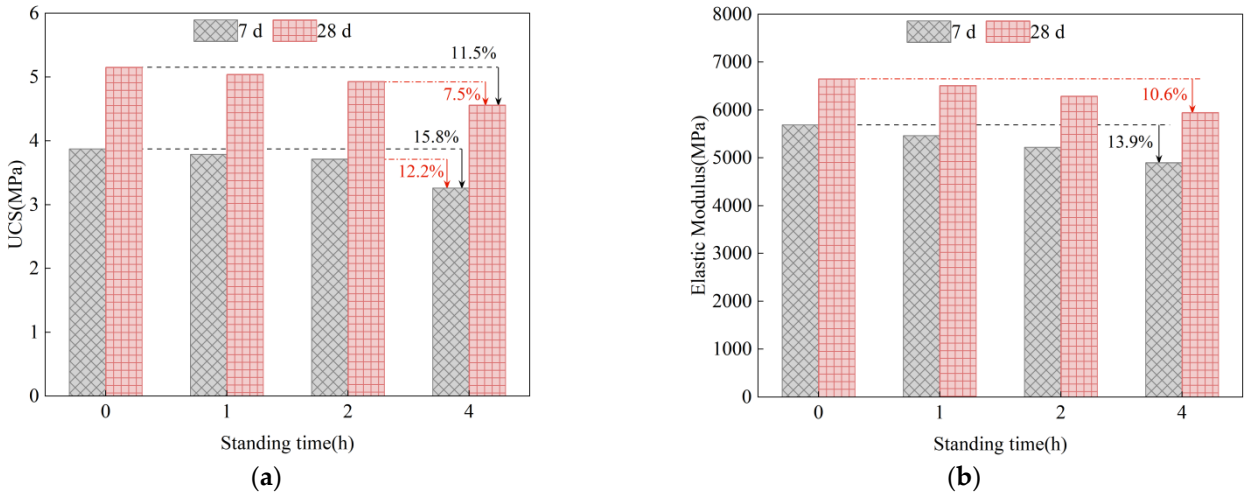


Figure 15. Effect of standing time on mechanical properties: (**a**) UCS, (**b**) elastic modulus.

The deterioration in mechanical properties is mainly associated with early cement hydration during standing and its subsequent effect on compaction. As hydration proceeds, the workability and particle rearrangement capacity of CCSG decrease, making it more difficult for subsequent compaction to form an aggregate skeleton as dense as that achieved by immediate compaction. Consequently, effective particle contact and interparticle restraint are weakened [37], leading to reductions in strength and stiffness. With increasing curing age, continued hydration partially improves interparticle bonding; therefore, the relative reductions in 28-day UCS and elastic modulus were generally smaller than those at 7 days. However, the adverse effects induced by delayed compaction could not be fully eliminated. Considering both mechanical indicators, the performance loss remained relatively limited when the standing time was within 2 h under the material composition and environmental conditions investigated in this study, whereas a marked deterioration was observed after 4 h. Accordingly, the interval between mixing and compaction should preferably be controlled within 2 h for the CCSG investigated in this study.

3.4.2. Curing Temperature

The 7-day and 28-day UCS and elastic modulus results at different curing temperatures are presented in Figure 16. As shown in Figure 16a,b, curing temperature had a pronounced effect on the mechanical properties of CCSG. With 20 °C curing taken as the reference condition, curing at 5 °C reduced the 7-day UCS from 3.87 to 2.83 MPa and the elastic modulus from 5687 to 4613 MPa, corresponding to reductions of 26.9% and 18.8%, respectively. These results indicate that low-temperature curing markedly suppresses the development of early-age strength and stiffness. At 35 °C, the 7-day UCS and elastic modulus increased to 4.28 MPa and 6072 MPa, respectively, representing increases of 10.5% and 6.8% relative to the 20 °C condition. This indicates that moderately elevated curing temperatures promote early-age mechanical development. With increasing curing age, the influence of curing temperature became less pronounced. At 28 days, curing at 5 °C reduced the UCS and elastic modulus by 12.6% and 10.7%, respectively, relative to 20 °C, whereas curing at 35 °C increased both indicators by only 1.2%. Thus, the adverse effect of low-temperature curing was partially alleviated with age but remained evident at 28 days, while the benefit of elevated temperature was concentrated mainly at early ages.

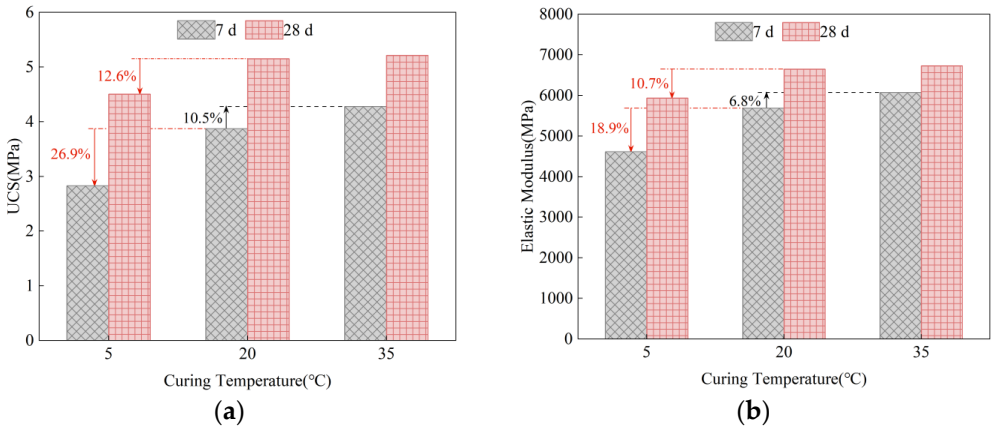


Figure 16. Effect of curing temperature on mechanical properties: (**a**) UCS, (**b**) elastic modulus.

Curing temperature influences mechanical development primarily by altering the hydration kinetics of the cementitious system. Relative to 20 °C, curing at 5 °C reduces cement hydration activity and delays the formation of hydration products and interparticle bonding structures [38], thereby suppressing early-age strength and stiffness. In contrast, the higher reaction rate at 35 °C accelerates hydration product formation [38,39], resulting in higher 7-day UCS and elastic modulus. As hydration progresses, however, the advantage of elevated temperature diminishes, and the mechanical properties of the 35 and 20 °C groups become nearly comparable at 28 days. Overall, curing at 20 °C provided relatively stable mechanical development, whereas enhanced thermal insulation is recommended during early-age curing under low-temperature construction conditions to mitigate performance loss.

3.4.3. Curing Mode

The 7-day UCS and elastic modulus results under different curing modes are presented in Figure 17. As shown in Figure 17a,b, OC reduced both the UCS and elastic modulus of CCSG at the same curing temperature. At 5 °C, OC decreased the 7-day UCS from 2.83 to 1.99 MPa and the elastic modulus from 4613 to 3728 MPa, corresponding to reductions of 29.7% and 19.2%, respectively. At 20 °C, the UCS and elastic modulus decreased from 3.87 MPa and 5687 MPa to 3.11 MPa and 4776 MPa, respectively, corresponding to reductions of 19.6% and 16.0%. These results indicate that OC adversely affects both strength and stiffness development, with greater performance loss at 5 °C than at 20 °C. Moreover, the reduction in UCS was consistently greater than that in elastic modulus, suggesting that strength was more sensitive to moisture-loss-induced deterioration in interparticle bonding.

The superior performance under SC can be attributed to reduced moisture loss, which maintains a more stable moisture environment for continued hydration and bonding development. In contrast, OC accelerates moisture loss from the specimen surface and interior, restricting subsequent hydration and weakening interparticle bonding. The greater deterioration observed under the combined 5 °C and OC condition indicates that low temperature and moisture loss have a compounded adverse effect on mechanical performance. Therefore, adequate moisture retention should be maintained during curing, and additional thermal insulation is recommended under low-temperature construction conditions to mitigate early-age performance loss.

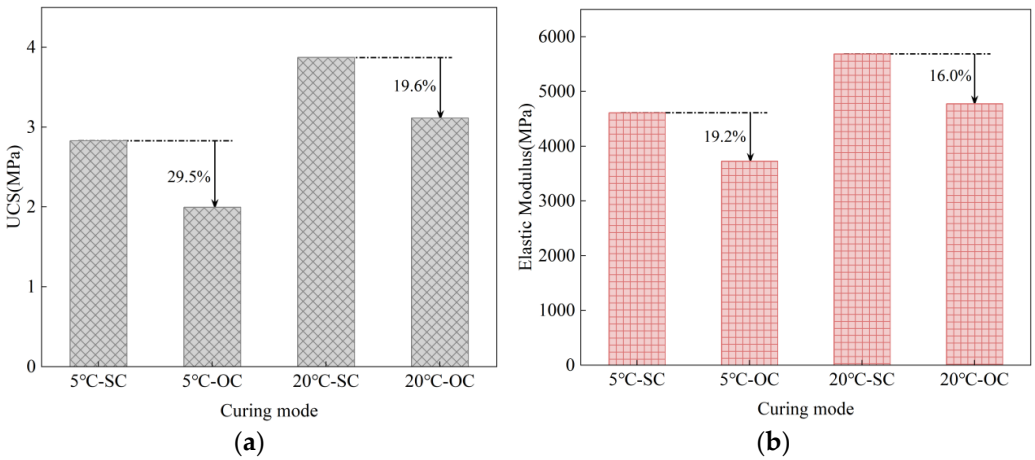


Figure 17. Effect of curing mode on mechanical properties: (**a**) UCS, (**b**) elastic modulus.

3.5. Microstructural Mechanisms

3.5.1. Aggregate-Binder Interfacial Morphology

To characterize the interfacial microstructural differences between CSG and CCSG containing untreated RAI, SEM was used to examine the distribution of hydration products, pore characteristics, and interparticle bonding. The results are presented in Figure 18.

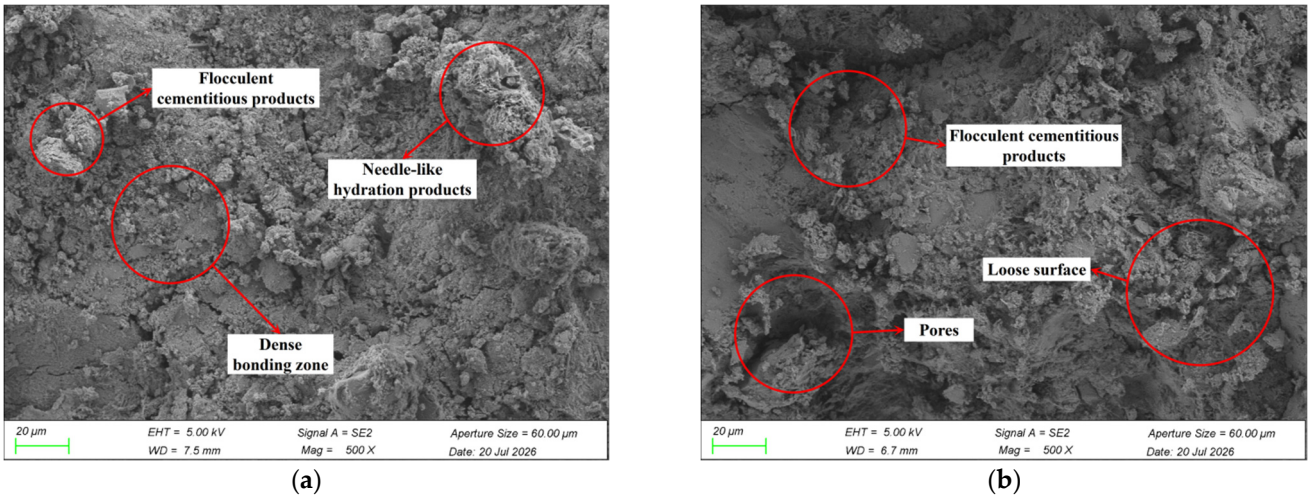


Figure 18. Microstructural characteristics of different aggregate systems: (**a**) cement-stabilized gravel, (**b**) cement-stabilized RAI.

As shown in Figure 18, abundant flocculent cementitious products and needle-like hydration products are distributed throughout the CSG matrix, locally interweaving to form dense bonding zones and relatively continuous particle-to-particle connections. In contrast, CCSG containing untreated RAI exhibits a less uniform distribution of cementitious products, with locally loose regions and residual pores. These features indicate that the adhered residual mortar and heterogeneous surface structure of RAI disrupt the continuous formation of newly generated hydration products and weaken local interfacial bonding, thereby reducing structural compactness [40]. The observed microstructural differences are consistent with the lower strength and stiffness of CCSG containing untreated RAI.

3.5.2. Interfacial Microstructure

To evaluate the changes in the RAI interfacial structure induced by different pretreatments, SEM images of untreated, A-treated, and APS-treated RAI were compared, as shown in Figures 18b and 19.

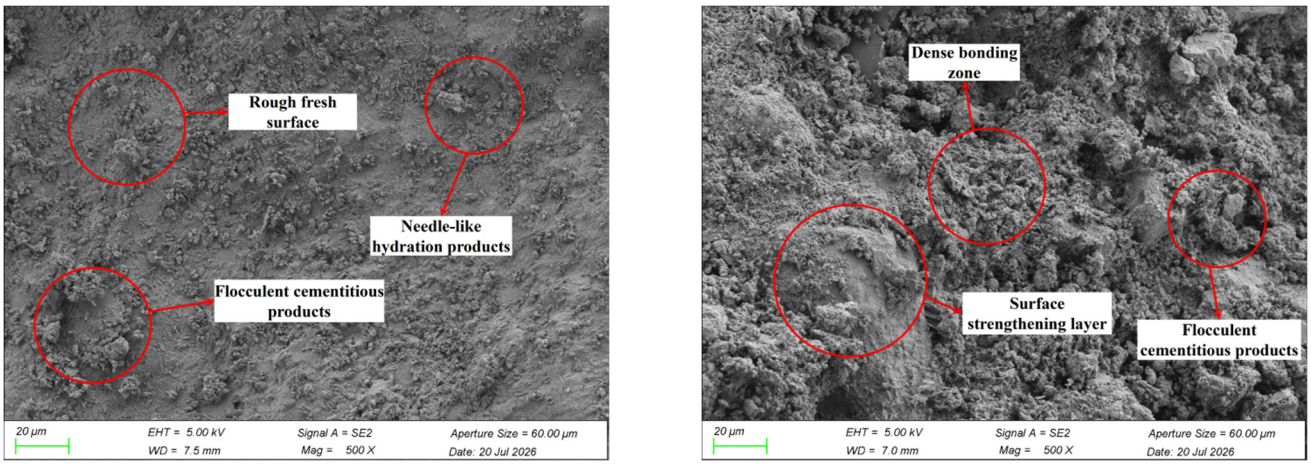


Figure 19. Microstructural characteristics of RAI interfaces under different pretreatment conditions: (**a**) A-treated group, (**b**) APS-treated group.

Untreated RAI exhibits locally loose surface regions and distinct pores, with relatively sparse flocculent cementitious products, indicating a heterogeneous local bonding structure associated with the adhered residual mortar, as shown in Figure 18b. After abrasion pretreatment, part of the loose and weakened adhered residual mortar is removed, exposing a rough fresh surface. More flocculent cementitious products and needle-like hydration products are subsequently observed, indicating that abrasion pretreatment improves the surface condition of RAI and provides a more favorable substrate for the attachment and growth of hydration products. After further pozzolanic slurry strengthening, a distinct surface strengthening layer is formed, accompanied by a more continuous distribution of cementitious products and locally dense bonding zones. These features indicate that the reaction products generated by the strengthening slurry coat and bond the RAI surface, producing a denser and more continuous interfacial structure [41].

Overall, abrasion pretreatment primarily removes the weakened surface layer and exposes a rough fresh surface, whereas pozzolanic slurry strengthening further improves the RAI surface through coating and secondary cementitious bonding. These microstructural changes are consistent with the increases in UCS, elastic modulus, and STS observed after pretreatment, confirming that improved surface condition and interfacial bonding are key mechanisms by which RAI pretreatment enhances the mechanical properties of CCSG.

3.5.3. Interfacial Phase Composition

To investigate the effects of different RAI pretreatments on crystalline phase composition and hydration reactions at the interface, XRD was used to identify the major phases and compare changes in their characteristic diffraction peaks. Representative phases were further evaluated semi-quantitatively, as shown in Figures 20 and 21.

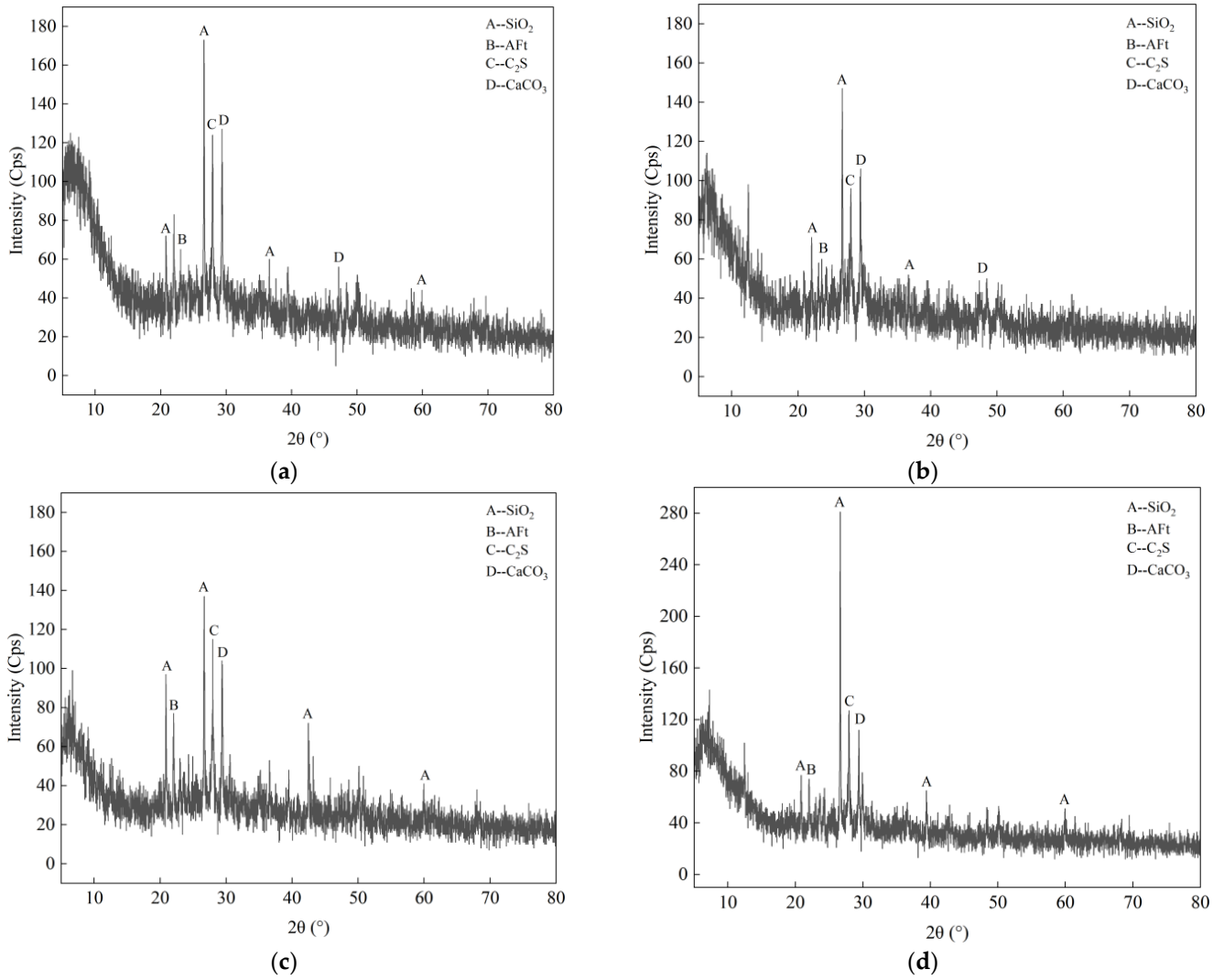


Figure 20. XRD patterns of interfacial products in different aggregate systems: (**a**) gravel, (**b**) untreated, (**c**) A-treated group, (**d**) APS-treated group.

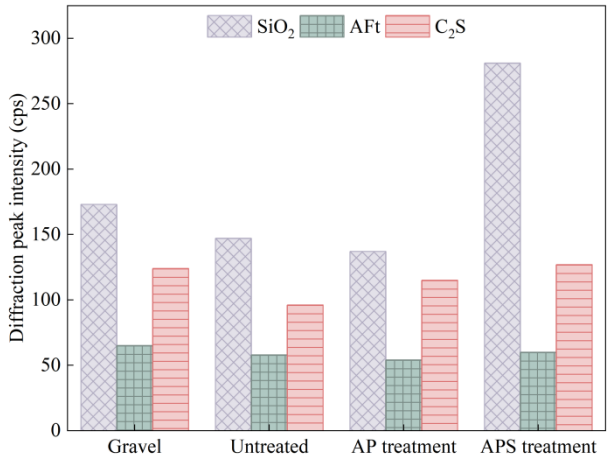


Figure 21. Representative crystalline-phase peak intensities in the interfacial transition zone.

As shown in Figure 20, the major diffraction peak positions of CSG, untreated RAI, A-treated RAI, and APS-treated RAI were generally consistent. Crystalline phases including SiO_2, AFt, C_2S, and $CaCO_3$ were identified in all groups, and no distinct new crystalline phases were detected. This indicates that RAI pretreatment did not substantially alter

the basic crystalline phase composition. Instead, the differences were mainly reflected in the relative intensities of characteristic peaks and in the contribution of poorly crystalline hydration products.

The XRD pattern of APS-treated RAI remained dominated by the original crystalline phases, although variations in the relative intensities of several characteristic peaks were observed, indicating that the pozzolanic slurry participated in interfacial reactions. Steel slag powder introduced residual calcium silicate phases such as C_2S, while reactive components in GGBFS further reacted under alkaline conditions, promoting the formation of poorly crystalline cementitious products [35]. Combined with the SEM observations of increased cementitious products and reduced interfacial pores and cracks after APS treatment, these results suggest that pozzolanic slurry strengthening improves interfacial continuity and bonding between RAI and the newly formed cementitious matrix through the formation of a denser cementitious coating layer.

As shown in Figure 21, the semi-quantitative analysis showed that the representative peak intensities of SiO_2, AFt, and C_2S in the CSG group were 173, 65, and 124 cps, respectively. In the untreated RAI group, the corresponding values decreased to 147, 58, and 96 cps, representing reductions of 15.03%, 10.77%, and 22.58% relative to the CSG group. This reduction may be associated with the adhered residual mortar, which dilutes the diffraction contribution of aggregate minerals and residual clinker phases and thereby lowers the corresponding characteristic peak intensities. After abrasion pretreatment, the representative peak intensities of SiO_2 and AFt decreased to 137 and 54 cps, respectively, corresponding to reductions of 6.80% and 6.90% relative to the untreated RAI group, whereas the C_2S peak intensity increased to 115 cps, representing an increase of 19.79%. These changes suggest that abrasion pretreatment removes part of the loose and weakened adhered residual mortar and surface hydration products, thereby increasing the relative diffraction contribution of exposed RAI minerals and residual clinker phases.

After pozzolanic slurry strengthening, the representative peak intensities of SiO_2, AFt, and C_2S increased to 281, 60, and 127 cps, respectively, corresponding to increases of 105.11%, 11.11%, and 10.43% relative to the A-treated group. The pronounced increase in the SiO_2 peak intensity is likely related to local enrichment of crystalline siliceous phases in the sampled region and may also reflect differences in sample packing and preferred orientation, as well as the introduction of silica-bearing constituents from the strengthening slurry. The moderate increases in the AFt- and C_2S-related peak intensities further suggest that steel slag powder and Al-bearing reactive components introduced by the slurry contribute to the crystalline phase assemblage within the interfacial region.

4. Conclusions

The effects of material composition, RAI pretreatment, and preparation and curing parameters on CCSG performance were evaluated. The main conclusions are as follows:

1. Increasing RAI content and RAP incorporation reduced the mechanical properties of CCSG. Without RAP, increasing RAI content from 0% to 90% reduced the 7-day UCS, elastic modulus, and STS by 30.34%, 21.29%, and 25.46%, respectively. At 4% cement content, approximately 30% RAI met the strength requirements for base-course applications, while higher contents were more suitable for subbase applications.

2. Both A and APS improved the mechanical performance of CCSG, with APS showing a stronger later-age effect. Compared with untreated CCSG, APS increased the 28-day UCS, elastic modulus, and STS by 63.67%, 37.27%, and 64.77%, respectively.

3. Standing time, curing temperature, and curing mode affected mechanical performance. After 4 h of standing, the 7-day UCS and elastic modulus decreased by 15.8% and 13.9%, respectively. Curing at 5 °C rather than 20 °C reduced them by 26.9% and 18.9%,

respectively. OC further impaired performance. For the mixtures investigated, the time between mixing and compaction should preferably not exceed 2 h, with adequate moisture retention and thermal insulation during early-age curing.

4. Untreated RAI exhibited locally loose surface regions and distinct pores. A treatment modified the RAI surface morphology, whereas APS formed a more continuous strengthening layer and denser interfacial bonding zones. The overall crystalline phase composition remained largely unchanged, suggesting that the strengthening effect was primarily associated with surface modification, improved interfacial bonding, and cementitious reactions.

The effects of recycled road aggregates on the mechanical properties and strength mechanism of cement-stabilized gravel were investigated in this study. The long-term durability of CCSG under freeze–thaw cycles, extreme temperature fluctuations and saline-alkali erosion will be explored to facilitate its large-scale application in cold and arid regions.

Author Contributions: Conceptualization, J.J. and X.Z.; methodology, L.C. and P.W.; writing—original draft preparation, J.J., L.C. and X.Z.; writing—review and editing, P.W., H.L. and C.W.; visualization, L.C.; supervision, P.W. and C.W.; project administration, J.J. and C.W.; funding acquisition, J.J., P.W. and C.W. All authors have read and agreed to the published version of the manuscript.

Funding: This research was funded by the Science and Technology Research and Development Project of Xinjiang Transportation Investment (Group) Co., Ltd. (grant number XJJTZKX-FWCG-202411-0737); the Transportation Industry Science and Technology Project of Xinjiang Uygur Autonomous Region (grant number 2024-ZD-002); the National Natural Science Foundation of China (grant number 52408457); the Natural Science Foundation of Xinjiang Uygur Autonomous Region (grant number 2026D01D06); and the China Postdoctoral Science Foundation (grant number 2025M771640).

Institutional Review Board Statement: Not applicable.

Informed Consent Statement: Not applicable.

Data Availability Statement: The data presented in this study are available on request from the corresponding author.

Conflicts of Interest: Authors Jianfeng Jia, Xuegang Zhang and Haiyan Li were employed by Xinjiang Transportation Investment (Group) Co., Ltd. and Xinjiang Transportation Investment Construction Management Co., Ltd., Urumqi, China. The other authors declare that the research was conducted in the absence of any commercial or financial relationships that could be construed as a potential conflict of interest.

References

1. Ma, T.; Luan, Y.-C.; He, L.; Huang, X.; Wang, S.; Wang, N.; Ma, Y. Review on cold recycling technology development of emulsified asphalt and foamed asphalt. *J. Traffic Transp. Eng.* **2023**, *23*, 1–23. [CrossRef]
2. Luan, Y.-C.; Chen, T.; Ma, T.; Ma, Y.; Wang, N. Fracture performance analysis of cold-recycled mixture based on DEM precise modeling. *China J. Highw. Transp.* **2021**, *34*, 125–134. [CrossRef]
3. Wen, L.; Liu, D.; Zhang, R.; Yang, X.; Xu, S.; Qiu, C.; Ji, J. A review of the composition, regeneration mechanism, and performance of cold recycled asphalt mixture. *J. Traffic Transp. Eng. (Engl. Ed.)* **2026**, *13*, 714–736. [CrossRef]
4. Wang, C.; Liu, J.; Zhang, X.; Wang, Y.; Chen, S. DEA-orthogonal collaborative optimization design of high-viscosity anti-slip resin-based chip seal material composition. *Constr. Build. Mater.* **2026**, *509*, 145171. [CrossRef]
5. Wen, P.; Fan, Z.; Chen, Q.; Ge, T.; Ding, L.; Wang, C. Application of X-ray computed tomography imaging in the digital modeling of asphalt mixtures: A state of the art review. *J. Road Eng.* **2026**, *6*, 332–363. [CrossRef]
6. Li, H.; He, S.; Dang, S.; Shang, A.; Ren, J.; Liu, Q.; Zhao, D.; Yang, F. Performance evaluation and optimization of emulsified asphalt cold recycled mixtures using dual-recycled RAP and RAI materials. *J. Road Eng.* **2026**, *6*, 148–159. [CrossRef]
7. Tataranni, P.; Sangiorgi, C.; Simone, A.; Vignali, V.; Lantieri, C.; Dondi, G. A laboratory and field study on 100% recycled cement bound mixture for base layers. *Int. J. Pavement Res. Technol.* **2018**, *11*, 427–434. [CrossRef]
8. Chakravarthi, S.; Boyina, A.; Singh, A.K.; Shankar, S. Evaluation of cement treated reclaimed asphalt pavement and recycled concrete pavement bases. *Int. J. Pavement Res. Technol.* **2019**, *12*, 581–588. [CrossRef]

9. Li, Q.; Wang, Z.; Li, Y.; Shang, J. Cold recycling of lime-fly ash stabilized macadam mixtures as pavement bases and subbases. *Constr. Build. Mater.* **2018**, *169*, 306–314. [CrossRef]
10. Zhang, Q.; Wei, H.W.; Wang, Y.B.; Ying, G.Q.; Hu, J.L. Experimental study on cement-stabilized cold recycled lime soil. *J. Xi'an Univ. Archit. Technol. (Nat. Sci. Ed.)* **2012**, *44*, 632–636.
11. Ji, X.; Jiang, Y.; Liu, Y. Evaluation of the mechanical behaviors of cement-stabilized cold recycled mixtures produced by vertical vibration compaction method. *Mater. Struct.* **2016**, *49*, 2257–2270. [CrossRef]
12. Jiang, Y.J.; Shen, B.; Chen, G.-X. Splitting strength properties of cement cold recycling mixtures based on vertical vibration compaction. *J. Chang'an Univ. (Nat. Sci. Ed.)* **2016**, *36*, 9–16, 58.
13. Xu, S.; Wang, Y.; Yin, J.; Yuan, Y.; Fang, L.; Jia, X. Study on composition design and strength characteristics of cement-stabilized cold recycled mixture materials. *Mater. Sci. Technol.* **2025**, *33*, 29–37. [CrossRef]
14. Xu, J.; Huang, S.; Qin, Y.; Li, F. The impact of cement contents on the properties of asphalt emulsion stabilized cold recycling mixtures. *Int. J. Pavement Res. Technol.* **2011**, *4*, 48–55.
15. Hu, Q.; Zhang, J.; He, Y.; Li, J.; Song, C.; Li, G. Investigation of mechanical properties, stiffness, and flexibility of cold recycled cement-stabilized gravel base milling mixes with foamed asphalt. *J. Mater. Civ. Eng.* **2023**, *35*, 04023443. [CrossRef]
16. Al-Ihekwaba, E.; Dave, E.V.; Sias, J.E. Properties and structural contributions of engineered emulsion stabilized cold recycled materials based on mixture composition variation. *Transp. Res. Rec.* **2025**, *2679*, 1–20. [CrossRef]
17. Jin, D.; Yin, L.; Malburg, L.; You, Z. Laboratory evaluation and field demonstration of cold in-place recycling asphalt mixture in Michigan low-volume road. *Case Stud. Constr. Mater.* **2024**, *20*, e02923. [CrossRef]
18. Wang, Y.; Liu, Y. Study on fatigue characteristics of cement cold recycled mixtures in seasonally frozen regions. *Bull. Chin. Ceram. Soc.* **2017**, *36*, 2415–2423, 2429.
19. Gao, Z.; Zhu, J.; Fang, L.; Li, X. Effects of hydroxypropyl methyl cellulose ether on the full-deep cold regenerated mixture stabilized with cement. *J. Univ. Shanghai Sci. Technol.* **2019**, *41*, 300–306. [CrossRef]
20. Liu, J.; Huang, L.; Li, X.; Shao, H. Effect of polypropylene fiber on properties of cold recycled mixture of water stabilized base course in alpine region. *J. Univ. Shanghai Sci. Technol.* **2021**, *43*, 460–467. [CrossRef]
21. Ren, J.; Wang, S.; Zang, G. Effects of recycled aggregate composition on the mechanical characteristics and material design of cement stabilized cold recycling mixtures using road milling materials. *Constr. Build. Mater.* **2020**, *244*, 118329. [CrossRef]
22. Zhao, Z.; Wang, S.; Ren, J.; Wang, Y.; Wang, C. Fatigue characteristics and prediction of cement-stabilized cold recycled mixture with road-milling materials considering recycled aggregate composition. *Constr. Build. Mater.* **2021**, *301*, 124122. [CrossRef]
23. Mou, G.; Shen, A.; Lyu, Z.; Wang, L.; Guo, Y.; Wei, Z.; Yin, L. Effect of early strength anti-cracking materials on drying shrinkage of recycled cement stabilized macadam. *Int. J. Pavement Eng.* **2023**, *24*, 2039922. [CrossRef]
24. Fedrigo, W.; Kleinert, T.R.; Núñez, W.P.; Graeff, Â.G.; Filho, L.C.P.d.S.; Brito, L.A.T. Shrinkage of cold recycled cement-treated mixtures of asphalt pavement materials. *J. Test. Eval.* **2023**, *51*, 2230–2244. [CrossRef]
25. Li, Y.; Zhao, L.; Gao, J.; Ru, Y.; Zhang, H. Evaluation of the fatigue performance of full-depth reclamation with Portland cement material based on the Weibull distribution model. *Coatings* **2024**, *14*, 437. [CrossRef]
26. Liu, H.; Ren, J.; Zhang, L.; Lv, Q.; Zhuang, S.; Zhao, H. Uncertainty quantification of fatigue life for cement-stabilized cold recycled mixtures using probabilistic programming. *Materials* **2025**, *18*, 4439. [CrossRef]
27. *JTG/T 5521-2019*; Technical Specifications for Highway Asphalt Pavement Recycling. China Communications Press: Beijing, China, 2019.
28. *JTG 3441-2024*; Technical Specifications for Construction of Highway Asphalt Pavements. China Communications Press: Beijing, China, 2024.
29. *JTG D50-2017*; Specifications for Design of Highway Asphalt Pavement. China Communications Press: Beijing, China, 2017.
30. Hou, K.; Hua, W.; Xiao, Y.; Wang, X.; Yang, T. Insights into the failure mechanisms of cement-treated recycled aggregate materials (CRAMs) under uniaxial compression via peridynamics. *Constr. Build. Mater.* **2024**, *451*, 138726. [CrossRef]
31. Qin, X.; Lin, Y.; Chen, S.; Sun, X.; Yang, X.; Huang, Q. Mechanical properties and repairing mechanism of recycled cement stabilized macadam for road base based on microbial induced carbonate precipitation technology. *Case Stud. Constr. Mater.* **2024**, *21*, e03516. [CrossRef]
32. Liu, M.; Hu, J.; Sun, J.; Li, Y.; Luo, S. Characterization of roadway epoxy asphalt binder with different epoxy contents. *J. Mater. Civ. Eng.* **2023**, *35*, 04023144. [CrossRef]
33. Brand, A.S.; Roesler, J.R. Bonding in cementitious materials with asphalt-coated particles: Part II—Cement-asphalt chemical interactions. *Constr. Build. Mater.* **2017**, *130*, 182–192. [CrossRef]
34. Behravan, A.; Lowry, M.; Ashraf-Khorasani, M.; Tran, T.Q.; Feng, X.; Brand, A.S. Effect of pretreatment on reclaimed asphalt pavement aggregates for minimizing the impact of leachate on cement hydration. *Cem. Concr. Res.* **2023**, *173*, 107305. [CrossRef]
35. Guo, L.; Liu, J.; Chen, D.; An, S. Mechanical properties and microstructure evolution of alkali-activated GGBS-fly ash-steel slag ternary cements. *Constr. Build. Mater.* **2024**, *444*, 137727. [CrossRef]

36. Shaban, W.M.; Elbaz, K.; Yang, J.; Thomas, B.S.; Shen, X.; Li, L.; Du, Y.; Xie, J.; Li, L. Effect of pozzolan slurries on recycled aggregate concrete: Mechanical and durability performance. *Constr. Build. Mater.* **2021**, *276*, 121940. [CrossRef]
37. Nazari, Z.; Tabarsa, A.; Latifi, N. Effect of compaction delay on the strength and consolidation properties of cement-stabilized subgrade soil. *Transp. Geotech.* **2021**, *27*, 100495. [CrossRef]
38. Hara, H.; Shirabe, Y. Strength estimation method for arbitrary age of cement-treated soil based on high-temperature curing history. *Soils Found.* **2023**, *63*, 101295. [CrossRef]
39. Cardone, F.; Grilli, A.; Bocci, M.; Graziani, A. Curing and temperature sensitivity of cement-bitumen treated materials. *Int. J. Pavement Eng.* **2015**, *16*, 868–880. [CrossRef]
40. Liu, J.; Ma, K.; Shen, J.; Zhu, J.; Long, G.; Xie, Y.; Liu, B. Influence of recycled concrete aggregate enhancement methods on the change of microstructure of ITZs in recycled aggregate concrete. *Constr. Build. Mater.* **2023**, *371*, 130772. [CrossRef]
41. Siletani, A.H.; Asayesh, S.; Shirzadi Javid, A.A.; Korayem, A.H.; Ghanbari, M.A. Influence of coating recycled aggregate surface with different pozzolanic slurries on mechanical performance, durability, and micro-structure properties of recycled aggregate concrete. *J. Build. Eng.* **2024**, *83*, 108457. [CrossRef]

Disclaimer/Publisher's Note: The statements, opinions and data contained in all publications are solely those of the individual author(s) and contributor(s) and not of MDPI and/or the editor(s). MDPI and/or the editor(s) disclaim responsibility for any injury to people or property resulting from any ideas, methods, instructions or products referred to in the content.